Free Radical Biology and Medicine 193 (2022) 9–22

Contents lists available at ScienceDirect

Free Radical Biology and Medicine

journal homepage: www.elsevier.com/locate/freeradbiomed

Cigarette smoke induces pulmonary arterial dysfunction through an imbalance in the redox status of the soluble guanylyl cyclase

J. Sevilla-Montero [a,1], O. Munar-Rubert [a,1], J. Pino-Fadón [a], C. Aguilar-Latorre [a], M. Villegas-Esguevillas [b,c], B. Climent [b,c], M. Agrò [d], C. Choya-Foces [e], A. Martínez-Ruiz [e], E. Balsa [d], C. Muñoz-Calleja [a], R.M. Gómez-Punter [f], E. Vázquez-Espinosa [f], A. Cogolludo [b,c], M.J. Calzada [a,c,*]

[a] Departamento de Medicina, Facultad de Medicina, Universidad Autónoma de Madrid. Instituto de Investigación Sanitaria Princesa (IIS-Princesa), Madrid, Spain
[b] Departamento de Farmacología y Toxicología, Facultad de Medicina, Universidad Complutense de Madrid, Madrid, Spain
[c] Centro de Investigación Biomédica en Red de Enfermedades Respiratorias (CIBERES), Instituto de Salud Carlos III, Madrid, Spain
[d] Departamento de Biología Molecular, Centro de Biología Molecular Severo Ochoa (CBMSO), Consejo Superior de Investigaciones Científicas (CSIC)-Universidad Autónoma de Madrid, Madrid, Spain
[e] Unidad de Investigación, Hospital Santa Cristina, Instituto de Investigación Sanitaria Princesa (IIS-Princesa), Madrid, Spain
[f] Servicio de Neumología, Hospital Universitario La Princesa, Instituto de Investigación Sanitaria Princesa (IIS-Princesa), Madrid, Spain

ARTICLE INFO

Keywords:
COPD
Cigarette smoke
Mitochondrial superoxide
NADPH oxidases
NRF2
sGC
Vasodilation
Pulmonary artery

ABSTRACT

Chronic obstructive pulmonary disease (COPD), whose main risk factor is cigarette smoking (CS), is one of the most common diseases globally. Some COPD patients also develop pulmonary hypertension (PH), a severe complication that leads to premature death. Evidence suggests reactive oxygen species (ROS) involvement in COPD and PH, especially regarding pulmonary artery smooth muscle cells (PASMC) dysfunction. However, the effects of CS-driven oxidative stress on the pulmonary vasculature are not completely understood. Herein we provide evidence on the effects of CS extract (CSE) exposure on PASMC regarding ROS production, antioxidant response and its consequences on vascular tone dysregulation. Our results indicate that CSE exposure promotes mitochondrial fission, mitochondrial membrane depolarization and increased mitochondrial superoxide levels. However, this superoxide increase did not parallel a counterbalancing antioxidant response in human pulmonary artery (PA) cells. Interestingly, the mitochondrial superoxide scavenger mitoTEMPO reduced mitochondrial fission and membrane potential depolarization caused by CSE. As we have previously shown, CSE reduces PA vasoconstriction and vasodilation. In this respect, mitoTEMPO prevented the impaired nitric oxide-mediated vasodilation, while vasoconstriction remained reduced. Finally, we observed a CSE-driven downregulation of the Cyb5R3 enzyme, which prevents soluble guanylyl cyclase oxidation in PASMC. This might explain the CSE-mediated decrease in PA vasodilation. These results provide evidence that there might be a connection between mitochondrial ROS and altered vasodilation responses in PH secondary to COPD, and strongly support the potential of antioxidant strategies specifically targeting mitochondria as a new therapy for these diseases.

1. Introduction

Chronic obstructive pulmonary disease (COPD), a pathology characterized by chronic bronchitis, emphysema, small airway obstruction and persistent respiratory symptoms, is strongly influenced by environmental agents, primarily cigarette smoking (CS) [1]. In addition, some COPD patients suffer pulmonary hypertension (PH), with characteristic pulmonary artery (PA) remodeling, vascular tone dysregulation, increased pulmonary artery pressure (PAP) and right ventricle alterations [2,3]. Curative therapies for COPD or PH are not available yet and a more comprehensive understanding of their underlying mechanisms is needed to develop new therapeutic approaches.

CS direct effects on the pulmonary vasculature are less characterized

* Corresponding author. Departamento de Medicina, Facultad de Medicina, Universidad Autónoma de Madrid, Instituto de Investigación Sanitaria Princesa (IIS-Princesa), Madrid, Spain.
E-mail address: mariajose.calzada@uam.es (M.J. Calzada).
[1] These authors contributed equally to this work.

https://doi.org/10.1016/j.freeradbiomed.2022.09.026
Received 31 March 2022; Received in revised form 5 September 2022; Accepted 22 September 2022
Available online 26 September 2022

Abbreviations

5-HT	serotonin
ACh	acetylcholine
ANOVA	analysis of variance
cDNA	complementary DNA
COPD	chronic obstructive pulmonary disease
CS	cigarette smoke
CSE	cigarette smoke extract
Cyb5R3	cytochrome *b*5 reductase 3
FCCP	carbonyl cyanide-*p*-trifluoromethoxyphenylhydrazone
hPASMC	human pulmonary artery smooth muscle cells
NAC	N-acetyl-cysteine
NO	nitric oxide
NOX	NADPH oxidase
NOXA1	NOX activator 1
NOXO1	NOX organizer 1
NRF2	nuclear erythroid-2 related factor 2
OCR	oxygen consumption rate
ODQ	1H-[1,2,4]oxadiazolo[4,3-a]quinoxalin-1-one
PA	pulmonary artery
PAP	pulmonary artery pressure
PASMC	pulmonary artery smooth muscle cells
PH	pulmonary hypertension
ROS	reactive oxygen species
RS	recording solution
SEM	standard error of the mean
sGC	soluble guanylyl cyclase
SMC	smooth muscle cell
SNP	sodium nitroprusside
SOD	superoxide dismutase
tBHQ	tert-butylhydroquinone
TMRM	tetramethylrhodamine methyl ester
$\Delta\psi_m$	mitochondrial membrane potential

compared to the damage produced on the airways, since vascular remodeling was thought to just be a consequence of alveolar hypoxia due to emphysema and airway obstruction. However, in patients with severe emphysema and airway obstruction, PAP only slightly correlates with hypoxemia and airflow limitation, and no correlation exists between PAP and emphysema severity [4,5]. Furthermore, media thickening is also observed in PA of mild COPD patients and smokers without airway obstruction [6]. This suggests that other unknown mechanisms, hypoxia-independent and directly triggered by CS on the pulmonary vasculature, may also be responsible for PH development in these patients [7]. In fact, we recently demonstrated that cigarette smoke extract (CSE) directly decreases PA vasoconstriction and vasodilation responses, with alterations intrinsic to the smooth muscle cell (SMC) layer which could contribute to CS-dependent PH development [8].

COPD development is closely related to oxidative stress, and increased oxidative stress markers have been observed in exhaled breath condensates [9–14], and lung tissue from COPD patients compared to control subjects [15–21]. It has been proposed that oxidative modifications in the lung may arise from CS and air pollutants themselves, such as acrolein [22]. This unsaturated aldehyde is known to transiently form protein adducts in human bronchial epithelial cells *in vitro*, and to acutely deplete GSH levels and inactivate thioredoxin reductase activity. However, endogenously-produced reactive oxygen species (ROS) also play an important role in COPD pathogenesis, where systems like NADPH oxidase (NOX), xanthine oxidase and mitochondrial respiration appear to be the most relevant ones [23]. In parallel, decreased antioxidant defenses are also linked to COPD and its exacerbations. This includes reduced glutathione availability [24], nuclear erythroid-2 related factor 2 (NRF2) downregulation [25,26], vitamins A and E depletion, and altered DNA repair mechanisms [27–29].

NOX family has been identified among the different endogenous sources of pulmonary ROS, with higher amounts of NOX2-expressing immune cells found within the lung of COPD patients [30], and NOX4 levels in airway epithelial and SMC correlating with COPD severity [31–33]. Interestingly, pulmonary artery smooth muscle cells (PASMC) from COPD patients also have higher NOX4 levels [34], although if this arises from CS impact or hypoxia contribution is unclear. Evidence suggests that CS might directly take a part on NOX-derived vascular oxidative stress, since rat aortic SMC show higher NOX1 levels responsible for increased superoxide production upon *in vitro* CSE exposure [35].

Mitochondrial respiratory chain complexes are important superoxide sources as well, releasing ROS towards the mitochondrial matrix or to the intermembrane space [36]. Mitochondrial damage induced by CS exposure in COPD leads to the accumulation of dysfunctional mitochondria in airway SMC with decreased ATP synthesis and increased ROS production rates [37], which may also play a key role in the vascular remodeling during COPD pathogenesis.

Cellular ROS levels are also delimited by a group of antioxidant enzymes regulated by transcription factor NRF2, encoded by *NFE2L2* gene [38]. Interestingly, a study on the association between *NFE2L2* gene polymorphisms and airflow insufficiency in smokers points out that defective NRF2 might play a role in COPD due to insufficient antioxidant, protective responses [39]. Additionally, decreased *NFE2L2* mRNA and NRF2 protein levels are detected in lung tissue, pulmonary macrophages and bronchial epithelium of COPD patients compared to healthy donors [26,40–42]. However, CSE can also drive NRF2 upregulation and nuclear translocation in human bronchial epithelial cells *in vitro* [43–45], which would argue against CS disrupting NRF2 pathway. Therefore, the role of NRF2 in COPD-related PH could be more complex than what is already stablished.

ROS, and specifically superoxide, can react with nitric oxide (NO) to produce peroxynitrite [46], thus scavenging NO and diminishing its downstream effects in the vasculature. CS effects on pulmonary NO pathway are mostly characterized in terms of decreased NO production [47–49] and endothelium-dependent PA vasodilation [50–52]. However, direct effects of CS on PA tunica media regarding this pathway are not fully understood, and evidence suggesting additional dysfunction of soluble guanylyl cyclase (sGC) or other downstream effectors in SMC are still unclear. Functional sGC is a heterodimer of α and β subunits, where sGCβ subunit binds a heme cofactor with a Fe^{2+} ion, sensitive to NO [53] only in this reduced form, in comparison to the oxidized Fe^{3+} state which cannot coordinate to NO [54]. Cytochrome *b*5 reductase 3 (Cyb5R3) has been identified as responsible for maintaining this Fe^{2+} state of sGC in vascular SMC [55], and mice lacking SMC *Cyb5r3* expression show higher arterial pressure values and are more sensitive to angiotensin-driven hypertension [56]. Compounds increasing sGC activity are grouped into two main families with different pharmacological properties: stimulators (such as riociguat and BAY 41–2272, which upregulate sGC activity when the heme group is in its reduced, Fe^{2+} state) and activators (like ataciguat or cinaciguat, which promote sGC activity on its oxidized and even heme-free forms) [57]. sGC stimulators have shown some benefits preventing right ventricle hypertrophy and vascular muscularization in preclinical models of chronic CS exposure [58]. Nonetheless, since they also prevent emphysema and induce bronchodilation [58,59], NO-sGC pathway dysfunction still cannot be unequivocally assigned to hypoxia, CS or a combination of both.

In the present study, we analyzed the CSE *in vitro* effects related to oxidative stress accumulation and NO-sGC vasodilation pathway in

human PASMC. Particularly, we observed a CSE-mediated increase in mitochondrial superoxide levels, which was not accompanied by an upregulation of antioxidant enzymes. This mitochondrial ROS burden likely targets NO-sGC signaling pathway, which explains the prevention of CSE-mediated dysfunction in the presence of mitoTEMPO. Additionally, our results pointed to a significant downregulation of Cyb5R3, which might promote an excessive oxidation of the sGC, as suggested by PA vasodilation being diminished in response to riociguat and conversely augmented in response to ataciguat and cinaciguat.

2. Materials and methods

2.1. Cell culture

Primary human pulmonary artery smooth muscle cells (hPASMC) were obtained from ScienCell Research Laboratories (#3110). Cells were cultured, following manufacturer's recommended specifications, in SMC complete medium (ScienCell, #1101) containing 2% fetal bovine serum (ScienCell, #0010), 1X SMC growth supplement (ScienCell, #2352 and #1152), 100 U/mL penicillin and 100 μg/mL streptomycin (ScienCell, #0503). Cells were used for a maximal number of 8 passages and were maintained at 37 °C in a humidified atmosphere of 5% CO_2.

2.2. Cigarette smoke extract (CSE) preparation

CSE was prepared from commercial Marlboro Red cigarettes (Philip Morris Brand Sàrl Neuchâtel, Switzerland, 13 mg tar and 1.0 mg nicotine/cigarette [60]). The smoke from the complete consumption of five cigarettes was continuously bubbled into 150 mL of PBS using VACUSAFE aspiration system (INTEGRA Biosciences AG) at a vacuum pump flow rate of 8 L/min. CSE solution was filtered through a 0.20 μm-pore system, immediately aliquoted and kept at −80 °C until used. To ensure a similar preparation amongst different batches, CSE concentration was measured spectrophotometrically at 320 nm wavelength. This solution was considered to be 100% CSE and diluted to obtain the desired concentrations for each experiment. To avoid the exposure to volatile substances from the smoke, untreated and CSE-challenged cells were always kept in different incubators.

2.3. RT-PCR analysis

Cells were grown to 90% confluence in 100 mm plates in the presence or absence of CSE for 24 h and total RNA was isolated using TRI Reagent (Molecular Research Center Inc., TR118). RNA (1 μg) was reverse transcribed to complementary DNA (cDNA) with MultiScribe™ Reverse Transcriptase (Applied Biosystems, 4308228) in a final volume of 20 μL cDNA (1 μL) was amplified with the specific primer pairs presented in Table 1 at a final 1 μM concentration and quantitative PCR was performed using GoTaq® qPCR Master Mix (Promega, A6001). Data were analyzed by the $2^{-\Delta Ct}$ method using StepOne Plus Software (Applied Biosystems) and all values were controlled with *HPRT1* gene expression levels and normalized to arbitrary units among different replicates.

2.4. Western blot analysis

Cells were grown to 90% confluence in 6-well plates in the presence or absence of CSE for 24 h and lysates were prepared in non-reducing 2X Laemmli buffer, boiled at 95 °C for 10 min in the presence of 20 mM DTT, electrophoretically separated by SDS-PAGE and transferred onto 0.45-μm nitrocellulose membranes (GE Healthcare Life Sciences, 10600003). Total protein bands were reversibly stained with Fast Green FCF (Sigma, F7252) and imaged on ImageQuant LAS 4000 or Amersham ImageQuant 800 (GE Healthcare Life Sciences) for total protein quantification. Transferred proteins were probed overnight at 4 °C with specific primary antibodies (Table 2). Horseradish peroxidase-conjugated secondary antibodies (anti-mouse IgG, Dako, P0260, and anti-rabbit IgG, Invitrogen, 32460) were added for 1 h at room temperature and protein signal was then visualized using Immobilon Forte (Millipore, WBLUF0500) on ImageQuant LAS 4000 or Amersham ImageQuant 800. Specific protein bands intensity was quantified by densitometry using ImageJ 1.51 software (U. S. National Institutes of Health, Bethesda, Maryland, USA) and normalized to the intensity of Fast Green FCF staining from each complete gel lane.

Table 2
List of antibodies used for Western blot and their corresponding product information.

Target protein	Clonality (clone)	Host species	Manufacturer (catalog number)
SOD2	Monoclonal (mAbcam74231)	Mouse	Abcam (ab74231)
SOD1	Monoclonal (24)	Mouse	Santa Cruz (sc-101523)
SOD3	Monoclonal (4G11G6)	Mouse	Abcam (ab80946)
catalase	Monoclonal (A-4)	Mouse	Santa Cruz (sc-271358)
NRF2	Monoclonal (383727)	Mouse	R&D Systems (MAB3925-SP)
α-tubulin	Monoclonal (DM1A)	Mouse	Sigma (T9026)
H2A	Monoclonal (L88A6)	Mouse	Cell Signaling Technology (3636)
NOX1	Polyclonal	Rabbit	Novus (NBP1-31546)
NOX4	Polyclonal	Rabbit	Novus (NB110–58849SS)
p22phox	Polyclonal	Rabbit	Abcam (ab75941)
NOXA1	Monoclonal (H-6)	Mouse	Santa Cruz (sc-398873)
NOXO1	Monoclonal (F-5)	Mouse	Santa Cruz (sc-390927)
sGCα	Polyclonal	Rabbit	Abcam (ab50358)
sGCβ (Western blot)	Polyclonal	Rabbit	Sigma (SAB4501344)
sGCβ (co-IP)	Polyclonal	Rabbit	Cayman Chemical (160897)
Cyb5R3	Polyclonal	Rabbit	ProteinTech (10894-1-AP)

Table 1
List of primers and their corresponding sequences used in RT-PCR analyses.

Target gene	Encoded protein	Forward primer sequence (5' – 3')	Reverse primer sequence (5' – 3')
NOX1	NOX1	TCACCAATTCCCAGGATTGA	TGTGGTCTGCACACTGGAAT
NOX4	NOX4	TGCAGCAAGATACCGAGATG	GTGATCATGAGGAATAGCAC
CYBA	$p22^{phox}$	AAGAGGAAGAAGGGCTCCAC	GAGAGCAGGAGATGCAGGAC
NOXA1	NOX activator 1 (NOXA1)	CATGATGCCAGGTCCCTAAT	CTCTGCTCCTGGTAGGCAGT
NOXO1	NOX organizer 1 (NOXO1)	GGTCCCCAGTTCTGTGCTT	CGGTCTGACGTTTCCAACAC
HMOX1	heme oxygenase 1	CGTTCCTGCTCAACATCCAG	GGGGCAGAATCTTGCACTTT
HPRT1	hypoxanthine phosphoribosyl transferase 1	ATTGTAATGACCAGTCAACAGGG	GCATTGTTTTGCCAGTGTCAA

2.5. Mitochondrial mass and mitochondrial superoxide levels quantification

Mitochondrial mass levels and specific mitochondrial superoxide levels were quantified with the fluorescent probes MitoTracker™ Green FM (ThermoFisher Scientific, M7514) and MitoSOX™ Red (ThermoFisher Scientific, M36008). Following 24-h treatment with CSE in the absence or presence of 25 nM mitoTEMPO (Sigma, SML0737), cells were incubated with DMSO as vehicle control, or with 25 nM MitoTracker™ Green FM and 5 μM MitoSOX™ Red, in HBSS for 15 min at 37 °C. Afterwards, cells were trypsinized and median MitoTracker™ Green FM and MitoSOX™ Red fluorescence was measured on a FACSCanto II cytometer (BD Biosciences) illuminating with Ar 488 nm laser and excluding cell debris and doublets from the analysis. Specific changes in MitoTracker™ Green FM and MitoSOX™ Red signal intensities were quantified by subtracting fluorescence from DMSO-treated hPASMC and normalized to arbitrary units among different replicates.

2.6. Mitochondrial oxygen consumption

Oxygen consumption rate (OCR, pmol O_2/min) of hPASMC was measured using Seahorse XF96 metabolic analyzer and Seahorse XF Cell Mito Stress Test kit (103015-100, Seahorse XF Technology, Agilent), following manufacturer's recommendations. Cells ($3{\cdot}10^4$ hPASMC per well) were seeded onto XF96 V3 PS Cell Culture Microplates (101085-004, Agilent) and exposed to air or CSE for 24 h before being loaded into the analyzer. OCR was monitorized over time while 5 μM oligomycin, 0.5 μM carbonyl cyanide-*p*-trifluoromethoxyphenylhydrazone (FCCP) and 2 μM rotenone plus 5 μM antimycin A from Mito Stress Test kit were sequentially added to the cells. Mitochondrial respiration-related parameters where quantified in terms of OCR as follows: basal respiration (OCR prior to oligomycin addition minus OCR after rotenone/antimycin A addition), H^+ leakage (OCR prior to oligomycin addition minus OCR after oligomycin addition), maximal respiratory capacity (OCR after FCCP addition minus OCR after oligomycin addition), ATP-linked respiration (basal respiration minus H^+ leakage OCR) and spare capacity (maximal capacity minus basal respiration). Data was normalized by cell density using Cytation 5 Cell imaging reader (Biotek Instruments), using Hoechst (ThermoFisher Scientific) as nuclear staining.

2.7. Cytosolic and nuclear subcellular fractionation

For cytosolic and nuclear protein fractions isolation, NE-PER™ Extraction Reagent (Pierce, 78833) was used following manufacturer recommendations. Cells were grown to 90% confluence in 100 mm plates in the presence or absence of CSE for 24 h (two 100 mm plates per condition). As a NRF2 stabilization positive control, some cells were instead challenged with 20 μM tert-butylhydroquinone (tBHQ). Afterwards, cells were trypsinized and split for both total protein lysate analysis and cytosolic/nuclear extraction using NE-PER™ kit. Total, cytosolic and nuclear fractions were solubilized in RIPA buffer and protein content was analyzed by bicinchoninic acid assay (ThermoScientific, 23225), prior to their analysis by Western blot. Cytosolic and nuclear fractions purity was assessed by α-tubulin and H2A histone levels determination, respectively.

2.8. Total superoxide levels quantification

Total superoxide levels were quantified using dihydroethidium (DHE) probe (ThermoFisher Scientific, D1168) in cells that had been challenged to CSE in the presence or absence of 15 mM N-acetyl-cysteine (NAC) (Sigma, A0737) for 24 h. Following this challenge, cells were incubated with DMSO as vehicle control, or with 10 μM DHE, in HBSS for 20 min at 37 °C. After that, cells were trypsinized, washed and DHE fluorescence was measured on a FACSCanto II (BD Biosciences) cytometer illuminating with an Ar 488 nm laser and excluding cell debris and doublets from the analysis. Specific changes in DHE signal intensity were quantified by subtracting fluorescence from DMSO-treated hPASMC, and normalized to arbitrary units among different replicates. In some experiments, cells were challenged to NOX inhibitor VAS2870. For those experiments, cells were treated for 24 h with 15% CSE and afterwards 10 μM VAS2870 was added for 10 min before DHE staining.

2.9. Mitochondrial network image analysis

Mitochondrial network morphology was assessed transfecting hPASMC grown on a 60 mm plate to 50% confluence with 1 μg pDsRed2-mito expression vector (Clontech Laboratories, 632421) and 2 μL Lipofectamine™ 2000 (ThermoFisher Scientific, 11668027). 24 h after transfection, hPASMC were trypsinized, allowed to attach on 10 μg/mL fibronectin-functionalized 13-mm glass coverslips and challenged with CSE in the presence or absence of mitoTEMPO for 24 h. Following CSE treatment, cells were fixed with 4% paraformaldehyde (Electron Microscopy Sciences, 15710) in PBS for 10 min at room temperature and mounted on slides in Faramount Aqueous Medium (Dako, S3025). Cells were imaged with a Leica DMR microscope using an immersion 100x objective (HCX PL APO 100X/1.40–0.7 oil CS, Leica) and illuminated with a mercury lamp (ebq 100, Lightning & Electronics JENA). Ten images per sample were collected using Leica DCF360FX camera and LAS V4.1 software, and mitochondrial network was analyzed following the previously described computational strategy [61], using ImageJ 1.51 software. Images were pre-processed by means of unsharp masking (radius = 3 pixels), local contrast enhancing and median filtering (radius = 2 pixels) and, afterwards, a binary mask of every image was generated to measure the area covered by mitochondrial signal (mitochondrial footprint) and to generate a skeletonized representation of the network. This skeletonized image was characterized in terms of the number of individual mitochondria, number of networks (containing at least one junction pixel), mean length of network branches and mean number of branches per network. Number of individual mitochondria and networks parameters were normalized over the mitochondrial footprint from the same image.

2.10. Mitochondrial membrane potential ($\Delta\psi_m$) assessment

Following 24-h exposure to CSE in the absence or presence of mitoTEMPO, $\Delta\psi_m$ in hPASMC was measured using the fluorescent probe tetramethylrhodamine methyl ester (TMRM, ThermoFisher Scientific, T7668), following the staining method described by Creed and McKenzie [62]. Cells were seeded on 8-well chambered coverslips (ThermoScientific, 155411) and stained with 20 nM TMRM and 2 μg/mL Hoechst 33342 in recording solution (RS, 109 mM NaCl, 50 mM KCl, 2 mM $MgSO_4$, 1.25 mM KH_2PO_4, 10 mM D-glucose, 2 mM $CaCl_2$ and 10 mM Hepes) for 40 min at 37 °C. Afterwards, cells were imaged on a Leica SP5 confocal microscope in the presence of 20 nM TMRM in RS using an immersion 40x objective (HCX PL APO CS 40X/1.25 oil UV, Leica) and illuminating with 488 nm Ar and 561 nm diode-pumped solid-state lasers. Cells were continuously recorded for 5 min before adding 10 μM FCCP (Sigma, C2920) to induce complete $\Delta\psi_m$ depolarization for an additional 5-min lapse. Confocal images were collected using Leica TCS SP5 software (Leica Microsystems, Mannheim, Germany). Subsequent analysis was performed on ImageJ 1.51, subtracting TMRM-channel background by means of rolling ball filtering method (radius = 50 pixels) and quantifying mean TMRM fluorescence intensity of every cell along time, from at least 10 cells per condition.

2.11. ATP levels quantification

Total ATP levels were quantified using Luminescent ATP Detection Assay Kit (ab113849, Abcam) following manufacturer's recommendations. After hPASMC challenge to CSE in the absence or presence of mitoTEMPO, cells were lysed for 5 min and luciferin-luciferase solution

was added during an additional 5-min time lapse. Following this incubation, luminescence was registered on a Glomax microplate reader (Promega), and ATP concentration was extrapolated from a reference curve of known ATP standard dilutions. Results were normalized by total protein determination using bicinchoninic acid assay (ThermoScientific, 23225).

2.12. Vascular contractility measurement

Animals were maintained at Medicine School animal facility of Universidad Autónoma of Madrid, kept under standardized conditions, and provided with standard diet and water *ad libitum*. PA from WT C57BL/6J mice were carefully dissected free of surrounding tissue, cut into rings (1.8–2 mm length) and overnight-exposed to 10% CSE in the presence or absence of 25 nM mitoTEMPO. Afterwards, vessel segments were mounted on a wire myograph in the presence of Krebs physiological solution. Contractility was recorded by an isometric force transducer and a displacement device coupled with a digitalization and data acquisition system (PowerLab, Paris, France). Preparations were firstly stimulated by rising the K^+ concentration of the buffer to 80 mM in exchange for Na^+. Vessels were washed three times and allowed to recover before a new stimulation. Arteries were then stimulated with increasing concentrations of serotonin (5-HT, from 10^{-8} to $3{\cdot}10^{-5}$ M, Sigma), endothelium-dependent vasodilator acetylcholine (ACh, from 10^{-9} to 10^{-5} M, Sigma) and NO donor sodium nitroprusside (SNP, from 10^{-11} to 10^{-5} M, Sigma). To evaluate sGC redox status, following PA vasoconstriction induction with 10^{-5} M 5-HT, vasodilation responses to increasing concentrations of the sGC stimulator riociguat or sGC activators ataciguat and cinaciguat (from 10^{-9} to 10^{-5} M) were evaluated. A minimum of four mice were used in these experiments, with at least two technical replicas from each one of them.

All animal experiments and procedures were conducted in accordance with the guidelines of the European Community Council Directive (86/609/EEC) and the Spanish Royal Decree 53/2013 based on the European Union normative (2010/63/UE). The Committee for Research and Ethics of the Universidad Autónoma de Madrid (PROEX 322/14) approved all protocols.

2.13. Co-immunoprecipitation (co-IP)

Cells were grown in a p150 plate at 95% confluency and treated with 15% CSE for 24 h. In parallel, other cells were also co-treated with 10 μM 1H-[1,2,4]oxadiazolo[4,3-a]quinoxalin-1-one (ODQ) for 10 min, as a positive control of sGCβ oxidation, or with mitoTEMPO 25 nM for 24 h. Cells were then lifted with trypsin and fixed with 1% paraformaldehyde for 10 min. Fixation was stopped with two washes of 1.25 M and 0.1 M glycine, and finally cells were lysated with NP-40 buffer (50 mM Tris/HCl, 150 mM NaCl, 2 mM EDTA, 1% NP-40) for 20 min at 4 °C. Protein G-Sepharose 4 Fast Flow (GE Healthcare) was bound to anti-sGCβ-1 antibody (Cayman Chemical, see Table 2) or to unspecific IgG (Mouse IgG2b, SA5-10266, Invitrogen) for 2 h at 4 °C. Cell lysates (500 μL) were incubated with 50 μL of Protein G-Sepharose for 4 h at 4 °C. Sepharose was centrifuged and supernatant was discarded, then protein was dissociated from Sepharose with Laemmli buffer at 95 °C for 10 min and afterwards analyzed by Western blot.

2.14. Statistical analysis

All data are presented as the mean ± standard error of the mean (SEM). For all the analyses, normality condition was evaluated using Shapiro-Wilk's test and, according to its results, subsequent analysis of the data was conducted as follows. On the one hand, if normality condition could be assumed, parametric statistical tests were used. When comparing the mean of two groups unpaired two-tailed Student's *t*-test was used, and when comparing the mean of a group and reference value, two-tailed one-sample Student's *t*-test was used. Alternatively, when comparing the means of three or more groups, one or two-way analysis of variance (ANOVA) tests followed by Bonferroni's pairwise comparisons were used. Finally, repeated measures ANOVA test followed by Bonferroni's *post hoc* pairwise comparisons was used to compare the means of three or more non-independent groups. On the other hand, if normality condition was not accomplished, non-parametric statistical tests were used, and Kruskal-Wallis' *H* test followed by Dunn's *post hoc* pairwise correction was used when comparing the medians of three or more groups. A p-value $P < 0.05$ was considered statistically significant. All the statistical analyses were performed on GraphPad Prism 7.0 software (San Diego, CA, USA).

3. Results

3.1. CSE exposure results in increased mitochondrial superoxide levels and reduced antioxidant defenses in PASMC

Recent results from our laboratory indicate that CSE increases intracellular superoxide levels in human PA fibroblasts and hPASMC [8], although the source of ROS in these cells is still unknown. Since one of the main vascular superoxide sources described in the lung and the pulmonary vasculature are the NOX complexes, we studied the expression of NOX1 and NOX4 enzymes and other additional subunits that contribute to their activity (namely $p22^{phox}$, NOXO1 and NOXA1) in hPASMC challenged to CSE. Although the mRNA levels of the various subunits were slightly increased after the treatment with CSE (Supplementary Fig. 1) compared to 0% CSE-exposed hPASMC, we did not observe a parallel increase at the protein level. Furthermore, following CSE-exposure we observed a statistically significant downregulation of $p22^{phox}$ protein, the subunit anchoring both functional NOX1 and NOX4-containing complexes to the cell membranes (Fig. 1A).

To explore other ROS sources, we also characterized the mitochondrial contribution to oxidative stress in hPASMC challenged with CSE, and measured mitochondrial superoxide levels by means of by MitoSOX™ staining and flow cytometry. We observed a significant increase in mitochondrial superoxide levels from the first hour of treatment and lasted for at least 24 h (Supplementary Fig. 2A and Fig. 1B, left). This increase was not accompanied by an increment in total mitochondrial mass, as measured by MitoTracker™ staining (Fig. 1B, right). Most importantly, our results proved a significant CSE-mediated downregulation on mitochondrial superoxide dismutase (SOD) 2 protein levels in hPASMC (Fig. 1C), which might further contribute to increase mitochondrial superoxide levels.

Next, we studied the effects of CSE in the electron transport chain, as the major source of mitochondrial ROS. We quantified hPASMC mitochondrial respiration rate by means of Seahorse assays to address if this mitochondrial superoxide accumulation would be associated to a dysfunction of this organelle. Our data suggested that CSE induced a significant decrease of hPASMC mitochondrial respiration following CSE exposure, as quantified in terms of a reduction in the oxygen consumption rates (OCR) associated to basal respiration, ATP-linked respiration, maximal respiration and spare capacity when compared to non-CSE exposed hPASMC (Fig. 1D).

Next, we assessed if CSE challenge compromised global antioxidant responses besides SOD2 downregulation. While no changes in cytosolic SOD1 levels were found, our results proved that CSE significantly diminished extracellular SOD3 and catalase enzymes (Supplementary Fig. 2B). To further characterize this anomalous cell behavior against a supposedly pro-oxidant stimulus like CSE, we considered evaluating if this was due to alterations in the levels or transcriptional activity of NRF2 in hPASMC after 15% CSE exposure. However, our results showed that NRF2 nuclear accumulation could indeed be taking place in CSE-challenged hPASMC compared to control, unexposed ones (Supplementary Fig. 2C). This nuclear accumulation seemed to promote NRF2 transcriptional activity, as we also observed induction of its target gene *HMOX1* (Supplementary Fig. 2D). Interestingly, other target genes such

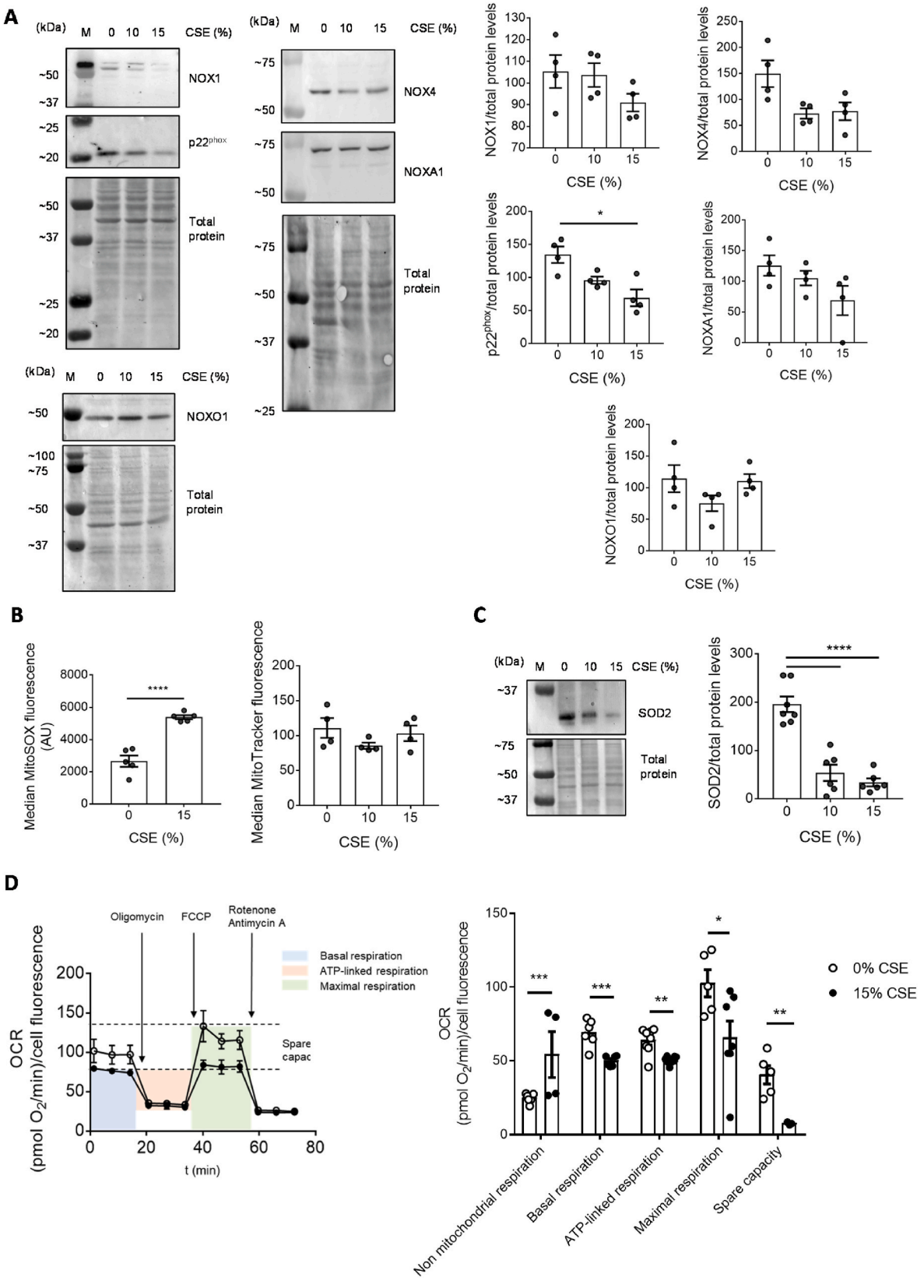

(caption on next page)

Fig. 1. Impact of CSE on NOX subunits, mitochondrial superoxide, SOD2 enzyme levels and mitochondrial respiration functions. Following 24-h challenge with CSE at the indicated concentrations, NOX subunits and SOD2 levels in hPASMC were analyzed by Western blot; mitochondrial superoxide levels and mitochondrial mass were analyzed by flow cytometry, and mitochondrial respiration was analyzed in terms of oxygen consumption rates (OCR). **A.** Protein levels of hPASMC were analyzed by Western blot probed against NOX1, $p22^{phox}$, NOX4, NOXA1, NOXO1 and total protein. Representative images (left) and band quantifications by densitometry (right) are shown. M: molecular weight marker lane. Densitometry data were controlled with total protein staining as loading control, normalizing arbitrary units among different replicates, and presented as mean ± SEM; n = 4. Statistical comparisons between groups were made using one-way ANOVA test followed by Bonferroni's *post hoc* test (*$P < 0.05$). **B.** Mitochondrial superoxide (left) and mitochondrial mass (right) levels were quantified using 5 μM MitoSOX™ and 25 nM MitoTracker™ probes, respectively. Values were calculated as the median fluorescence intensity of MitoSOX™ or MitoTracker™-stained cells minus the median fluorescence intensity of unstained cells, normalized to arbitrary units among different replicates and presented as mean ± SEM; n = 4. Statistical comparisons among groups were made using two-tailed one-sample Student's *t*-test (left) or Kruskal-Wallis' *H* test followed by Dunn's *post hoc* test (right) (****$P < 0.001$). **C.** Protein levels of hPASMC were analyzed by Western blot and probed against SOD2 and total protein. A representative image (left) and band quantifications by densitometry (right) are shown. M: molecular weight marker lane. Densitometry data were controlled with total protein staining as loading control, normalizing arbitrary units among different replicates, and presented as mean ± SEM; , n = 4–6. Statistical comparisons among groups were made using one-way ANOVA test followed by Bonferroni's *post hoc* test (****$P < 0.001$). **D.** Mitochondrial respiration functions of hPASMC treated with 0% or 15% CSE for 24 h were analyzed quantifying OCR values along time (left). Basal respiration, ATP production, maximal respiration and spare capacity values (right) were calculated from OCR measurements over cell amount and presented as mean ± SEM; n = 4–6. Statistical comparisons between both groups were made using two-tailed Student's *t*-test for all five variables (*$P < 0.05$, **$P < 0.01$, ***$P < 0.005$).

as SODs or catalase were not induced (data not shown). These results indicate that other non-transcriptional mechanisms might be involved in the reduced antioxidant response observed in our cells.

3.2. Mitochondrial superoxide scavenger mitoTEMPO reduces CSE-driven mitochondrial fission in hPASMC

Our data pointed towards a dysfunctional oxidative phosphorylation being included among the different effects exerted by CSE on hPASMC, resulting in the overproduction of superoxide free radical. Thus, this superoxide might contribute to the phenotype of aberrant vasoactive responses of the PA that we have previously observed following CS exposure [8]. Since the treatment with the antioxidant N-acetyl-cysteine (NAC) diminished the CSE-mediated increase of total ROS in our cells (Supplementary Fig. 3A), we also assessed mitochondria-targeted antioxidants to evaluate if this approach could also be valid in the context of pulmonary vascular cells. To this aim, hPASMC were incubated with CSE in the presence or absence of mitochondrial superoxide scavenger mitoTEMPO and total or mitochondrial superoxide were quantified. As expected, treatment with mitoTEMPO significantly attenuated the CSE-mediated increase on mitochondrial superoxide in these cells, while no effects on total superoxide were observed (Supplementary Fig. 3B). In agreement with our results from Fig. 1A suggesting that NOX are not involved in CSE-meditated increase of ROS, the increase of total ROS quantified with DHE was not attenuated in the presence of the NOX inhibitor VAS2870 (Supplementary Fig. 3C).

Mitochondrial fission and fusion dynamics are fundamental cell strategies to continuously self-renew dysfunctional mitochondria upon exogenous stress insults. CSE is known to induce fragmentation of the mitochondrial network within airway SMC and epithelial cells resulting from an abnormal balance between fusion and fission mechanisms [63–65]. To analyze the morphological effects that CSE had on hPASMC mitochondrial network, and whether they could be reverted with mitoTEMPO treatment, given the positive effect that mitoTEMPO had on reverting mitochondrial superoxide burden, we first transiently transfected the cells with a vector encoding for mitochondria-targeted DsRed2 protein. CSE-treated cells expressing this fluorescent protein showed a distinctive distribution throughout their mitochondrial networks (Fig. 2A). This allowed us to image and transform these networks onto binary, skeletonized shapes (Supplementary Fig. 4), and describe them in terms of individualized or network-forming mitochondria, as well as quantify the percentage of image covered by DsRed2 signal (namely, mitochondrial footprint), the average length of network-forming branches and, finally, the average number of branches per mitochondrial network. Using this image analysis tool, we compared the effects of CSE and mitoTEMPO onto hPASMC mitochondria. Data showed that CSE induced mitochondrial network fragmentation (Fig. 2A, left, white arrows), resulting in a significant increase in the number of individualized mitochondria (Fig. 2A, right), together with a slight increase in the number of mitochondrial networks as well (Fig. 2A, right). Although average length of the different branches did not significantly change upon CSE-challenge, networks in general were comprised of a lesser number of branches compared to non-CSE-exposed cells (Fig. 2A, right). Globally, all four parameters were compatible with a situation where, with no apparent changes in total mitochondrial mass, this was being restructured and preferentially relocated on individualized mitochondria rather than connected, fused networks. Interestingly, mitoTEMPO partly reverted some of these CSE-driven effects on the mitochondrial network morphology, especially on the amount of individualized and network-forming mitochondria (Fig. 2A, right).

3.3. MitoTEMPO protects hPASMC from mitochondrial membrane depolarization caused by CSE

Beyond these morphological criteria, we aimed to further analyze the protective effects of mitoTEMPO, characterizing hPASMC mitochondria from a functional point of view. Given our observations of reduced mitochondrial respiration rate upon CSE treatment, we hypothesized that this would translate into abnormal mitochondrial membrane potential ($\Delta\psi_m$) values and associate with reduced ATP levels. Therefore, after CSE exposure in the absence or presence of mitoTEMPO, we quantified $\Delta\psi_m$ status using life-imaging of tetramethylrhodamine methyl ester (TMRM)-stained hPASMC (Fig. 2B). As expected, CSE significantly induced a mitochondrial depolarization on hPASMC, as shown by reduced TMRM fluorescence compared to non-exposed cells (Fig. 2B). Interestingly, and congruent with a less fragmented, healthier mitochondrial network, mitoTEMPO induced a significant recovery of this decreased $\Delta\psi_m$ due to CSE exposure (Fig. 2B).

Finally, we wondered if this change in $\Delta\psi_m$ induced in hPASMC challenged to CSE affected the ATP cellular pool. Although our results did not reach statistical significance, they pointed towards a slight decrease in ATP levels upon acute CSE exposure (Fig. 2C), which agrees to what our indirect Seahorse measurements suggested.

3.4. MitoTEMPO reverts CSE-driven PA vasodilation decrease, but does not recover normal vasoconstriction responses

After showing that mitochondrial superoxide scavenger mitoTEMPO could indeed prevent some of the mitochondrial dysfunctions triggered by CSE in hPASMC *in vitro*, we then addressed the repercussions this could have on the PA functionality. If these alterations affecting the mitochondria network in hPASMC were mainly responsible for the lack of contractile force that CSE exerted on the PA and that we previously observed [8], it could be reasonable to expect that mitoTEMPO might alleviate part of this stiffened phenotype. Following *ex vivo* exposure of murine PA, we observed that CSE blunted vasoconstriction responses

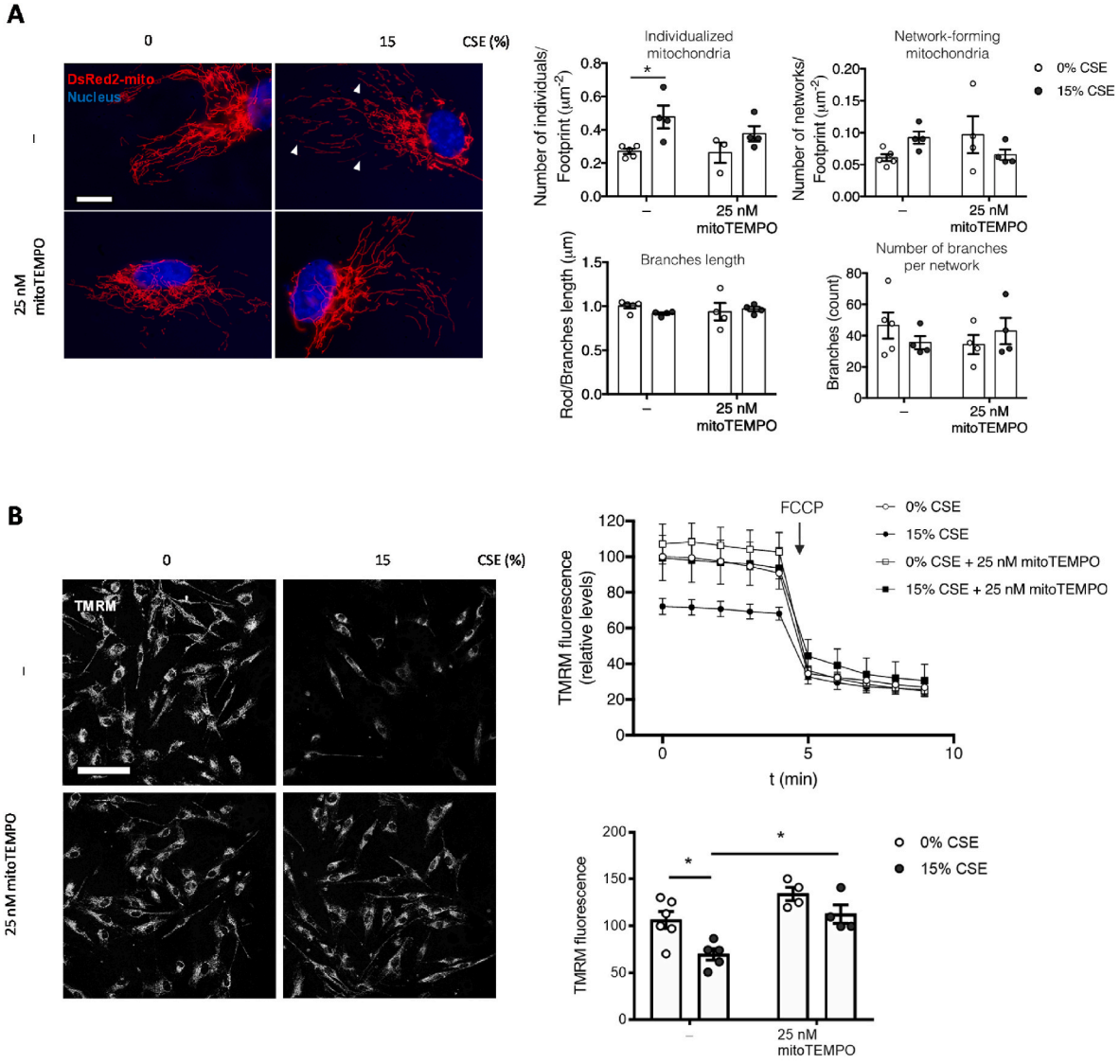

(caption on next page)

Fig. 2. Effects of mitoTEMPO treatment on CSE-triggered mitochondrial network fragmentation and $\Delta\psi_m$ depolarization in hPASMC. Following 24-h challenge with CSE in the absence or presence of 25 nM mitoTEMPO, hPASMC mitochondrial network morphology, mitochondrial membrane potential ($\Delta\psi_m$) values and total ATP levels were analyzed. **A.** Left: representative images of pDsRed2-mito transfected hPASMC, showing merged DsRed2-mito (red) and Hoechst (blue) signals, scale bar = 10 μm. White arrowheads indicate fragmented mitochondrial networks. Right: individualized and network-forming mitochondria values normalized over the surface covered by pDsRed2-mito signal (mitochondrial footprint) are shown, together with the quantification of the mean length of the branches within networks and average number of branches per network. All values are presented as mean ± SEM; n = 3–5. Statistical comparisons among groups were made using two-way ANOVA test followed by Bonferroni's *post hoc* test (*$P < 0.05$). **B.** Left: Confocal life-imaging was used to quantify $\Delta\psi_m$ in hPASMC stained with 20 nM TMRM; representative images are shown, scale bar = 100 μm. Right: TMRM fluorescence intensity values were calculated for 5 min before and 5 min after 10 μM FCCP addition, as $\Delta\psi_m$ depolarization positive control, from a minimal number of 10 cells per condition. Values were presented as mean ± SEM; n = 5–7 (top). Statistical comparisons of only the first TMRM intensity value among groups were made using two-way ANOVA test followed by Bonferroni's *post hoc* test (*$P < 0.05$) (bottom). **C.** Total ATP levels were quantified by chemiluminescence and normalized over total protein amount quantified by bicinchoninic acid assay. Values are presented as mean ± SEM; n = 3–4. Statistical comparisons were made using two-way ANOVA test followed by Bonferroni's *post hoc* test. (For interpretation of the references to colour in this figure legend, the reader is referred to the Web version of this article.)

both to KCl and serotonin (5-HT) and to a similar extent both in the absence and presence of mitoTEMPO (Fig. 3A). However, mitoTEMPO did show beneficial effects upon recovering the CSE-driven loss of PA vasodilation capacity on ACh-induced, endothelium-dependent vasodilation (Fig. 3B, left). Most importantly, mitoTEMPO also recovered endothelium-independent vasodilation, triggered by SNP treatment (Fig. 3B, right). Thus, the reduction of mitochondrial superoxide levels by mitoTEMPO could help preventing, specifically at the tunica media level, some of the deleterious effects of CSE on the vasodilation response of the PA.

3.5. CSE treatment results in the downregulation of Cyb5R3 levels in hPASMC

Considering these previous results, we wondered if CSE-driven upregulation of mitochondrial superoxide could somehow interfere with the NO signaling through the sGC pathway, given that mitoTEMPO was able to restore PASMC sensitivity to the NO-donor SNP. Nonetheless, we observed that CSE did not produce a significant decrease of the levels of structural sGC subunits (Fig. 4A, left). It has been recently proven that sGC sensitivity to NO is regulated by Cyb5R3, which maintains the fundamental reduced status of the heme group in sGC, this allowing for proper NO signaling and downstream cGMP synthesis [55]. Our data showed that CSE produced a significant downregulation of Cyb5R3 protein levels (Fig. 4A, right). This could imply that, in a superoxide-enriched scenario such as the one resulting from CSE treatment, antioxidant systems in charge of keeping sGC redox status might be insufficient, and sGC may become less sensitive to endothelial NO as well as to NO-donors like SNP.

3.6. CSE-mediated increase on mitochondrial superoxide promotes sGC oxidation and diminishes PA vasodilation response to riociguat

Oxidative stress within PASMC might be closely related to the fundamental requirement of sGC heme group reduced status. Thus, we aimed to explore whether this CSE-mediated decrease on Cyb5R3 was associated to an imbalance in the redox status of the sGC, in favor of a more oxidized form. Taking into account the results published by Rahaman et al. [55], we analyzed the binding of Cyb5R3 to sGCβ subunit, which depends on the redox status of its heme group. To this aim, we treated our cells with CSE in the absence or presence of mitoTEMPO or with 1H-[1,2,4]oxadiazolo[4,3-a]quinoxalin-1-one (ODQ), as an oxidizing agent. Then we performed a pull down of the sGCβ to assess its binding to Cyb5R3. Our results showed that the binding of the reductase

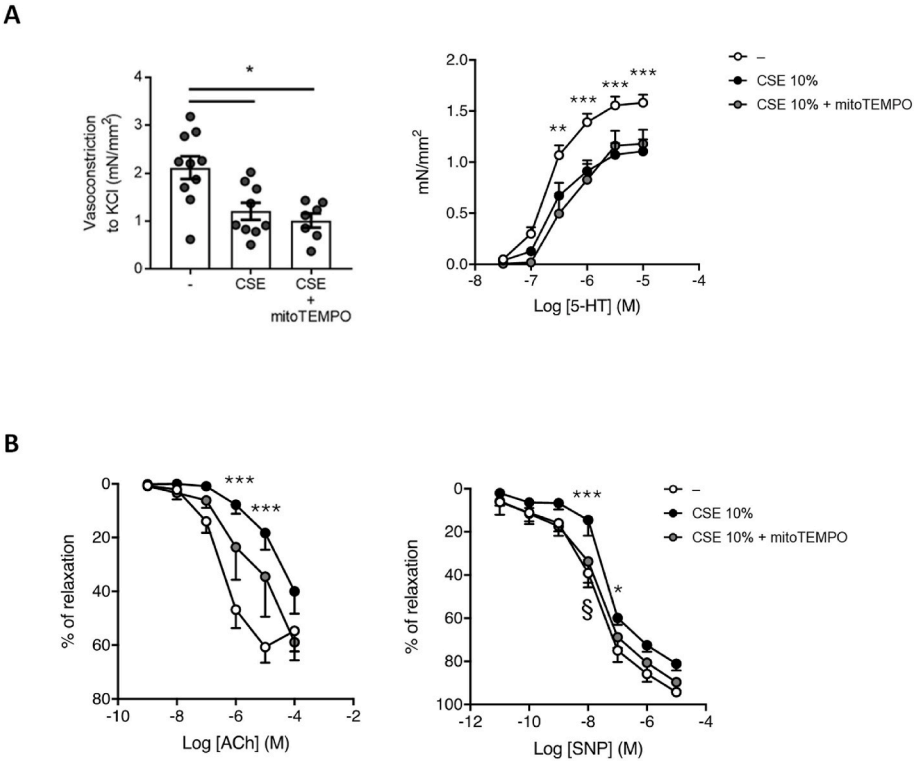

Fig. 3. Vasoconstriction and vasodilation responses of PA challenged to CSE and mitoTEMPO. Following overnight *ex vivo* challenge with 10% CSE in the absence or presence of mitoTEMPO, vascular responses of endothelium-intact PA from WT C57BL/6J mice were analyzed by wire myography. **A.** Vasoconstriction responses to 80 mM KCl (left) or to increasing concentrations of 5-HT (right) were presented as mean ± SEM; n = 7–10 mice. Statistical comparisons among groups were made using Kruskal-Wallis' *H* test followed by Dunn's *post hoc* test (left, *$P < 0.05$) or repeated measures two-way ANOVA test followed by Bonferroni's *post hoc* test (right, **$P < 0.01$, ***$P < 0.005$ between non CSE-exposed and CSE-exposed groups in the absence of mitoTEMPO). **B.** Vasodilation responses to increasing concentrations of acetylcholine (ACh, left) or sodium nitroprusside (SNP, right) were expressed as percentages of relaxation related to 10 μM 5-HT-driven vasoconstriction, and presented as mean ± SEM; n = 4–8 mice, each with at least two technical replicas. Statistical comparisons among groups were made using repeated measures two-way ANOVA test followed by Bonferroni's *post hoc* test (*$P < 0.05$, ***$P < 0.005$ between non CSE-exposed and CSE-exposed groups in the absence of mitoTEMPO; §$P < 0.05$ between CSE-exposed groups in the absence and presence of mitoTEMPO).

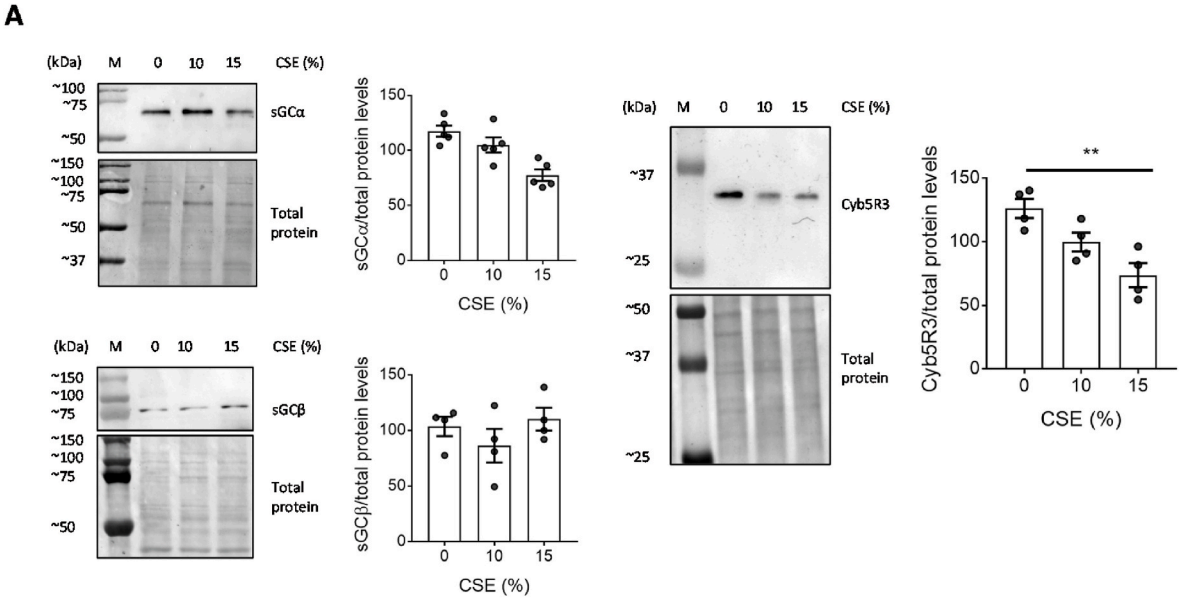

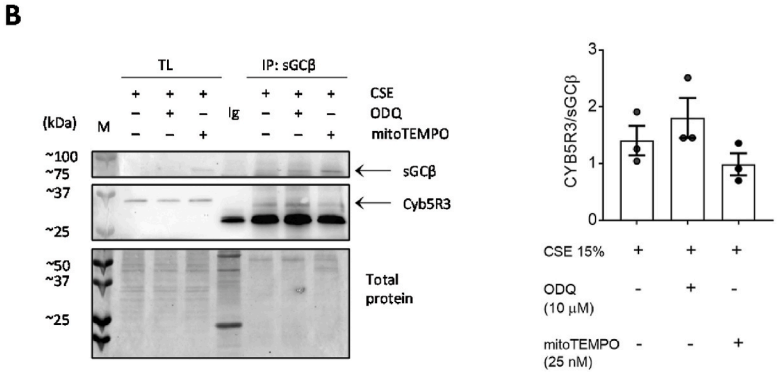

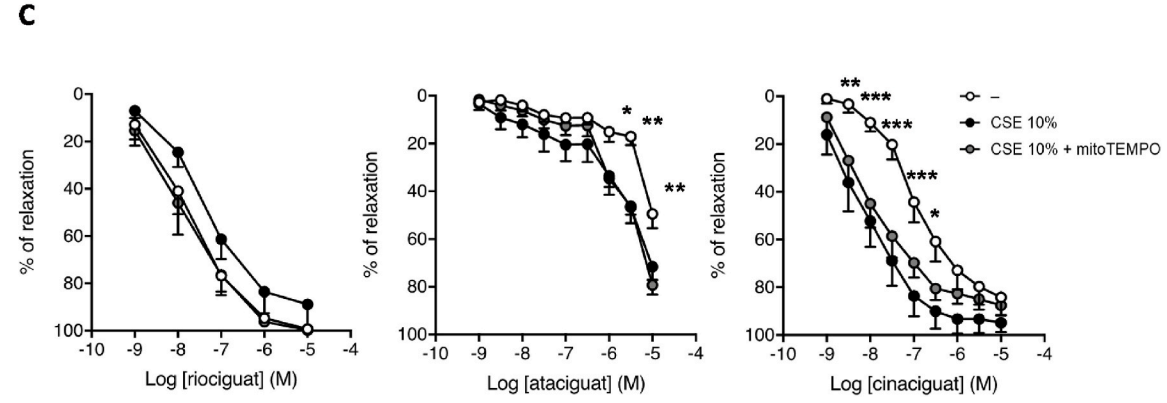

(caption on next page)

Fig. 4. CSE impact on sGC subunits and Cyb5R3 enzyme levels in hPASMC. Following 24-h challenge with CSE at the indicated concentrations, the expression of sGCα and sGCβ, subunits and reductase Cyb5R3 (**A**) in hPASMC was analyzed by Western blot. Representative images and band quantifications by densitometry are shown. M: molecular weight marker lane. Densitometry data were controlled with total protein staining as loading control, normalizing arbitrary units among different replicates, and presented as mean ± SEM; n = 4–5. Statistical comparisons among groups were made using one-way ANOVA test followed by Bonferroni's *post hoc* test (sGCα and sGCβ) or Kruskal-Wallis' *H* test followed by Dunn's *post hoc* test (Cyb5R3) (**$P < 0.01$). **B.** Following 24-h challenge with 15% CSE, cells were treated with 10 μM ODQ for 15 min or 25 nM mitoTEMPO for 24 h as indicated. sGCβ was purified from cell lysates with Sepharose by immunoprecipitation (IP) and then detected by Western blot probed against sGCβ and Cyb5R3. Total lysate (TL) samples prior to IP were analyzed together with unspecific IgG as negative control (Ig) and samples immunoprecipitated with anti-sGCβ IgG (IP: sGCβ). Representative images (left) and band quantifications by densitometry (right) are shown. M: molecular weight marker lane. Densitometry data were expressed as Cyb5R3 signal over sGCβ signal from the same lane and presented as mean ± SEM; n = 3. **C.** Following overnight *ex vivo* challenge with 10% CSE in the absence or presence of mitoTEMPO, vascular responses of endothelium-intact PA from WT C57BL/6J mice were analyzed by wire myography. Vasodilation responses to increasing concentrations of the sGC stimulator riociguat (left) or the sGC activators ataciguat (center) and cinaciguat (right) were expressed as percentages of relaxation related to 10 μM 5-HT-driven vasoconstriction and presented as mean ± SEM; n = 5–7. Statistical comparisons among groups were made using repeated measures two-way ANOVA test followed by Bonferroni's *post hoc* test (*$P < 0.05$, **$P < 0.01$, ***$P < 0.005$ between non CSE-exposed and CSE-exposed groups in the absence of mitoTEMPO).

to sGCβ was increased in hPASMC treated with CSE, or CSE + ODQ, compared to its binding in the presence of mitoTEMPO (Fig. 4B). This would indicate that, upon treatment with CSE, the sGC heme group might accumulate in an oxidized status, which would not be restored due to the drop in Cyb5R3 levels. Therefore, ROS-mediated oxidation of the sGCβ might promote an ineffective response to NO and thus a decrease in PA vasodilation.

To further support these results, we evaluated the PA vasodilation responses to the sGC stimulator riociguat and the sGC activators ataciguat and cinaciguat. Our results indicated that sGC excessive oxidation might indeed be occurring, since we observed a CSE-mediated reduction of PA vasodilation response to riociguat while the responses to ataciguat or cinaciguat were instead significantly increased (Fig. 4C). Interestingly, mitoTEMPO alleviated the CSE-driven reduced response to riociguat, whereas no clear changes in the response to ataciguat or cinaciguat were observed (Fig. 4C).

4. Discussion

COPD is a major health concern worldwide, and although the current therapies alleviate its symptoms, the disease is not definitely resolved. Therefore, it is necessary to unravel the mechanisms involved in COPD and COPD-related PH to design novel and effective treatments. Considering that oxidative stress is a major pathological trait of COPD [15–20], we tried to better decipher its contribution to the alterations we previously observed on PA and cells isolated from PA [8]. In this respect, it has been widely considered that alleviating oxidative stress could have a positive impact on the management of COPD patients, and therefore a revision of antioxidant treatments might enhance the benefits of currently approved vasodilation-targeted therapies. From a pharmacological perspective, this could widen the repertoire of molecular targets to address in COPD-related PH.

Our present results showed an increase in both total and mitochondrial superoxide levels in hPASMC challenged to CSE. However, we did not observe an increase in the levels of NOX protein after CSE treatment, which led us to think that the efficiency of these complexes to produce ROS was altered. Interestingly, it has been described that there is a redox crosstalk of mitochondrial ROS with NOX enzymes and an initial increase in cytosolic ROS levels is amplified by mitochondria [66,67]. This redox crosstalk might also be enhanced under conditions in which mitochondrial antioxidants defenses are decreased, as we observed in our CSE-treated cells. However, blocking mitochondrial ROS production with mitoTEMPO or using the NOX inhibitor VAS2870 did not alter CSE-mediated increase in ROS quantified with DHE, whereas VAS2870 proved effective in decreasing ROS levels in non-CSE-treated cells (Supplementary Fig. 3C). These data tell us that in terms of total ROS, neither NOX nor mitochondrial matrix superoxide (for which mitoTEMPO may function as a scavenger) contribute significantly, and therefore other systems could be possible sources of cytosolic ROS. It would be interesting to analyze the contribution of other enzymes such as xanthine oxidase and cytochrome P450 reductase, which also convert molecular oxygen to superoxide, in future studies. Additionally, the decrease on antioxidant activity could be explained in terms of *NFE2L2* mRNA downregulation, or insufficient NRF2 stabilization and nuclear translocation upon CSE treatment, as shown in COPD patients [26,40–42]. Nevertheless, our data pointed towards an increase in NRF2 nuclear accumulation and transcriptional activation of its target genes. However, we only observed induction of *HMOX1* mRNA, while mRNA levels for other genes like SODs and catalase were not induced (unpublished results). Thus, we cannot discard that a post-transcriptional regulation may occur and explain the decreased protein levels on these antioxidant enzymes, which affect the elimination of reactive species and therefore promote their accumulation in the cell when downregulated.

Related to the increase in mitochondrial superoxide levels, our experiments addressing mitochondrial network structure after CSE challenge suggested a dysfunctional, more fragmented network than in control hPASMC. Accordingly, Aravamudan et al. [64] also found a CSE-driven profound disruption of mitochondrial network in human airway SMC with increased fission-promoting dynamin-related protein 1 levels. Most importantly, in agreement with our own results in PASMC, these fragmented mitochondria also have higher superoxide levels and decreased respiration parameters, including ATP production. Similarly, hypoxia-driven mitochondrial alterations were recently shown on rat PASMC [68]. These authors demonstrate that hypoxia-driven fissioned mitochondria contribute to exert more vasoconstriction force and increased PAP, although, unfortunately, mitochondria energetics were not addressed. Nevertheless, these data suggest that although hypoxia may induce a similar mitochondrial network fragmentation compared to CSE, their repercussion onto PA contractility may not be identical.

Our recently published results demonstrate that supplementation with a high NAC concentration prevents CSE insults, particularly oxidative stress-triggered cell senescence induction [8]. Previous studies by Ito et al. demonstrate that treating human bronchial epithelial cells with mitoTEMPO effectively diminishes mitochondrial ROS production triggered by CSE and reduces the upregulation of senescence markers [69]. Furthermore, other authors have shown that ozone-mediated pulmonary damage is also reverted by diminishing oxidative stress with mitoTEMPO in mice [70]. In this same respect, other mitochondrial superoxide scavengers, such as mitoQ, have proven beneficial effects regarding age-related vascular dysfunction, improving aortic distensibility and flow-mediated vasodilation [71]. In our present study, we evaluated the antioxidant effects of mitoTEMPO on PA dysfunction and observed a partial amelioration of CSE-driven damage.

Together with ROS burden and fragmented mitochondrial network, our data showing decreased OCR and depolarized mitochondria might imply a CSE-driven deficient ATP production that might explain our recent published results (confirmed in this present study) in which CSE promotes the loss of contractile force at the PASMC level [8]. However, our present results only showed a modest decrease on total ATP levels due to CSE exposure, and mitoTEMPO did not prevent it. These results suggested that, because of the complex machinery needed for

contractility generation, additional alterations affecting Ca^{2+}-related signaling molecules, cytoskeleton proteins or ECM components might also contribute to this hypocontractile phenotype and therefore deserve a more systematic exploration in the future. Our preliminary results exploring the effects of CSE on cytoskeleton proteins suggested that CSE treatment decreased the phosphorylation of myosin light chains and altered the organization of actin filaments, which were shorter and more unstructured than in the control condition (unpublished results). Further studies would be interesting to explore these mechanisms and to clarify the contribution of CSE-driven oxidative stress to the decrease in PA vasoconstriction.

Like the effects on vasoconstriction, we wondered if mitochondrial ROS would also contribute to exacerbate the decrease in vasodilation that we observed. Our data showing that mitoTEMPO recovered PA sensitivity to endothelium-independent vasodilation inducers support this idea and could have several explanations worth exploring. On the one hand, excessive superoxide burden within PASMC likely targets NO-sGC vasodilator signaling pathway, because of the scavenging nature of superoxide on NO to form peroxynitrite [46]. This would not only diminish bioavailable NO for sGC activation but could also contribute to exacerbate oxidative stress on PASMC. Indeed, our results showing a CSE-driven SOD3 downregulation might indicate poor extracellular antioxidant defenses in the PA cells vicinity, which could therefore contribute to NO scavenging. On the other hand, an increase of oxidative stress within PASMC might be closely related to the fundamental requirement of sGC heme group reduced status. Our data demonstrate that the levels of the main enzyme maintaining this reduced form, Cyb5R3 [55], decreased following acute CSE challenge. In a pro-oxidant environment, this could translate onto an excessive sGC oxidation and, thus, diminished sensitivity to NO. This has actually been described in patients suffering from cerebral arteriopathy, whose vascular SMC indeed show significant sGC oxidation and reduced cGMP levels [72]. Our results indicated that this might in fact be the case, since we observed a better PA vasodilation response to the sGC stimulator riociguat in the presence of mitoTEMPO, this indicating that excessive mitochondrial superoxide burden within the PA prevented the vasodilation response due to an imbalance on the sGCβ heme redox status. This is important and support our previous results in which we observed that intraperitoneal treatment with NAC partially reversed CS-mediated decrease in contractility. However, this antioxidant had the opposite effect in the relaxation response to SNP [8]. Our present results are relevant and point out to the pharmacological benefits of vasodilation-related drugs in combination with specific sGC protection against the oxidative stress caused by CS, through mitochondrial ROS scavenging. In line with this, sGC activators might represent a preferred strategy compared to sGC stimulators under pathological conditions associated with enhanced sGC oxidation, such as chronic CS exposure.

5. Conclusions

In conclusion, our results demonstrate that CSE exposure causes an increase on superoxide levels in PASMC. We provide evidence of mitochondria as the most likely cellular source of increased superoxide. In addition, this study shows an inadequate antioxidant response in CSE-treated PASMC, thus suggesting that oxidative stress is a crucial mechanism which might have adverse effects in the pulmonary vasculature. Particularly, our data clearly show that CSE-challenged hPASMC display decreased levels of Cyb5R3 enzyme, which participates in maintaining sGC reduced status, needed for its NO-dependent activation (see our proposed model in the graphical abstract). Therefore, our results suggest that CSE-mediated increase of mitochondrial superoxide might contribute to compromise vascular responses in the PA. Given the increasing COPD burden nowadays, it is urgent to further characterize these pathways. The possible benefits of therapeutic strategies with the potential to alleviate mitochondrial oxidative stress in combination with stimulators of the NO-signaling pathway might be considered as a promising therapy for COPD-related PH recovery.

5.1. Limitations of the study

Our data support the relevance of mitochondrial ROS in human diseases such as COPD. However, an important limitation of our study concerns its eventual translation to human disease research, and the use of CSE alone as a model of CS exposure should be recognized and given special consideration. Adequately quantifying the exact chemical composition of CSE is not always a straightforward task and, therefore, there could be significant differences between this liquid mixture of components and the actual CS to which smokers are exposed. In the future, it would be interesting to better describe our CSE in terms of the presence and concentration of gases such as NO or CO, as well as reactive aldehydes such as acrolein or other prooxidant substances. The doses of these chemicals to which hPASMCs and murine PA were challenged in this study may or may not be comparable to those affecting the human lung while smoking. In this regard, there are also differences in the dose to which different individuals suffering from the disease are exposed, and therefore, it would be important to identify the minimum dose capable of contributing to the pathophysiology of COPD. Accordingly, a more realistic *in vivo* approach should also be undertaken to further demonstrate the role of CSE in mitochondrial ROS production, and whether drugs targeting this pathway could be considered for the design of clinical trials regarding the treatment of COPD or other respiratory pathologies. Finally, COPD is a tremendously heterogeneous disease with multiple risk factors, and CS is not the only underlying cause for its development. On the one hand, some COPD patients have never been smokers, and, on the other hand, COPD progression often continues even after smoking cessation, probably due to the hypoxia situation after the development of emphysema. This point was not addressed in our study since our aim was to characterize the effects at an early stage of the disease, prior to the development of the hypoxic environment within the lung. The possible reversibility or irreversibility of CSE-induced mitochondrial damage could also be further explored in the future, including the evaluation of whether these alterations we now describe are reversed once CSE is removed and the cells or vessels are allowed to recover.

Authors contribution

(1) the conception and design of the study, or acquisition of data, or analysis and interpretation of data (*S-M, J; P–F, J; M-R, O; V-E, M; C, B; A, M; C–F, C; C, A and C, MJ*)

(2) drafting the article or revising it critically for important intellectual content (*S-M, J; P–F, J; M-R, A; C, A; G-P, RM; V-E, E and C, MJ*)

(3) Manuscript revision (*S-M, J; M-R, O; A-L, C; M-R, A; C, A and C, MJ*)

(4) Final approval of the version to be submitted (*All authors*).

Role of the funding source

The Spanish Ministerio de Ciencia e Innovación, Programa Retos en Investigación (grant number PID2019-104406RB-100) **to MJC** provided the financial support for the conduct of the research included in this manuscript. Garantia Juvenil program from Comunidad de Madrid contributed with the research assistant contract to M-R, O.

Declaration of competing interest

We declare no competing interests.

Appendix A. Supplementary data

Supplementary data to this article can be found online at https://doi.org/10.1016/j.freeradbiomed.2022.09.026.

References

[1] Global Strategy for Diagnosis, Management and Prevention of C. 2021 GOLD Reports - Global Initiative for Chronic Obstructive Lung Disease - GOLD, 2021.
[2] M.C. Smith, J.P. Wrobel, Epidemiology and clinical impact of major comorbidities in patients with COPD, Int. J. COPD 9 (2014) 871–888.
[3] M. Humbert, et al., Pathology and pathobiology of pulmonary hypertension: state of the art and research perspectives, Eur. Respir. J. 53 (2019), 1801887.
[4] K. Chatterjee, A.R. Tarawneh, S. Alam, Out of proportion pulmonary hypertension in obstructive lung diseases, Curr. Opin. Pulm. Med. (2018) 24 161–172, https://doi.org/10.1097/MCP.0000000000000457, at.
[5] S.M. Scharf, et al., Hemodynamic characterization of patients with severe emphysema, Am. J. Respir. Crit. Care Med. 166 (2002) 314–322.
[6] S. Santos, et al., Characterization of pulmonary vascular remodelling in smokers and patients with mild COPD, Eur. Respir. J. 19 (2002) 632–638.
[7] J.A. Barberà, Mechanisms of development of chronic obstructive pulmonary disease-associated pulmonary hypertension, Pulm. Circ. 3 (2013) 160–164.
[8] J. Sevilla-Montero, et al., Cigarette smoke directly promotes pulmonary arterial remodeling and Kv7.4 channel dysfunction, Am. J. Respir. Crit. Care Med. 203 (2021) 1290–1305.
[9] K. Murata, et al., Hydrogen peroxide content and pH of expired breath condensate from patients with asthma and COPD, COPD 11 (2014) 81–87.
[10] P. Paredi, et al., Exhaled ethane, a marker of lipid peroxidation, is elevated chronic obstructive pulmonary disease, Am. J. Respir. Crit. Care Med. 162 (2000) 369–373.
[11] D. Makris, et al., Exhaled breath condensate 8-isoprostane, clinical parameters, radiological indices and airway inflammation in COPD, Respiration 75 (2008) 138–144.
[12] P.L. Paggiaro, et al., Malondialdehyde in exhaled breath condensate as a marker of oxidative stress in different pulmonary diseases, Mediat. Inflamm. (2011), 891752, 2011.
[13] N.L. Tateosian, et al., Inflammatory mediators in exhaled breath condensate of healthy donors and exacerbated COPD patients, Cytokine 58 (2012) 361–367.
[14] G.O. Osoata, et al., Peroxynitrite elevation in exhaled breath condensate of COPD and its inhibition by fudosteine, Chest 135 (2009) 1513–1520.
[15] E. Barreiro, et al., Oxidative stress and inflammation in the normal airways and blood of patients with lung cancer and COPD, Free Radic. Biol. Med. 65 (2013) 859–871.
[16] P.A. Kirkham, et al., Oxidative stress-induced antibodies to carbonyl-modified protein correlate with severity of chronic obstructive pulmonary disease, Am. J. Respir. Crit. Care Med. 184 (2011) 796–802.
[17] F.L.M. Ricciardolo, et al., Nitrosative stress in the bronchial mucosa of severe chronic obstructive pulmonary disease, J. Allergy Clin. Immunol. 116 (2005) 1028–1035.
[18] R. Gornati, et al., Protein carbonylation in human endothelial cells exposed to cigarette smoke extract, Toxicol. Lett. 218 (2013) 118–128.
[19] M. Yoshida, et al., Involvement of cigarette smoke-induced epithelial cell ferroptosis in COPD pathogenesis, Nat. Commun. 10 (2019) 3145.
[20] I. Rahman, et al., 4-Hydroxy-2-nonenal, a specific lipid peroxidation product, is elevated in lungs of patients with chronic obstructive pulmonary disease, Am. J. Respir. Crit. Care Med. 166 (2002) 490–495.
[21] E.G. Tzortzaki, et al., Oxidative DNA damage and somatic mutations: a link to the molecular pathogenesis of chronic inflammatory airway diseases, Chest 141 (2012) 1243–1250.
[22] M.J. Randall, M. Hristova, A. Van Der Vliet, Protein alkylation by the α,β-unsaturated aldehyde acrolein. A reversible mechanism of electrophile signaling? FEBS Lett. 587 (2013) 3808–3814.
[23] P.J. Barnes, Oxidative stress-based therapeutics in COPD, Redox Biol. 33 (2020), 101544.
[24] E.M. Drost, et al., Oxidative stress and airway inflammation in severe exacerbations of COPD, Thorax 60 (2005) 293–300.
[25] A.M. Fratta Pasini, et al., Oxidative stress and Nrf2 expression in peripheral blood mononuclear cells derived from COPD patients: an observational longitudinal study, Respir. Res. 21 (2020) 37.
[26] M. Suzuki, et al., Down-regulated NF-E2-related factor 2 in pulmonary macrophages of aged smokers and patients with chronic obstructive pulmonary disease, Am. J. Respir. Cell Mol. Biol. 39 (2008) 673–682.
[27] M.W. Schäffer, S.S. Roy, S. Mukherjee, S.K. Das, Vitamin A, vitamin E, lutein and β-Carotene in lung tissues from subjects with chronic obstructive pulmonary disease and emphysema, Open J. Respir. Dis. (2013) 44–51, 03.
[28] G. Caramori, et al., Unbalanced oxidant-induced DNA damage and repair in COPD: a link towards lung cancer, Thorax 66 (2011) 521–527.
[29] C.R. Sears, DNA repair as an emerging target for COPD-lung cancer overlap, Respir. Investig. 57 (2019) 111–121.
[30] C. Trocme, et al., Macrophage-specific NOX2 contributes to the development of lung emphysema through modulation of SIRT1/MMP-9 pathways, J. Pathol. 235 (2015) 65–78.
[31] F. Hollins, et al., Airway smooth muscle NOX4 is upregulated and modulates ROS generation in COPD, Respir. Res. 17 (2016) 84.
[32] B. Hao, et al., Nox4-derived ROS promotes collagen I deposition in bronchial smooth muscle cells by activating noncanonical p38MAPK/AKTmediated TGF-β signaling, Oxid. Med. Cell. Longev. 2021 (2021), 6668971.
[33] X. Liu, et al., The expression of NOX4 in smooth muscles of small airway correlates with the disease severity of COPD, BioMed Res. Int. 2016 (2016), 2891810.
[34] X. Guo, et al., NOX4 expression and distal arteriolar remodeling correlate with pulmonary hypertension in COPD, BMC Pulm. Med. 18 (2018) 111.
[35] K.H. Chang, et al., NADPH oxidase (NOX) 1 mediates cigarette smoke-induced superoxide generation in rat vascular smooth muscle cells, Toxicol. Vitro 38 (2017) 49–58.
[36] R.Z. Zhao, S. Jiang, L. Zhang, Z. Bin Yu, Mitochondrial electron transport chain, ROS generation and uncoupling (Review), Int. J. Mol. Med. 44 (2019) 3–15.
[37] H. Hara, K. Kuwano, J. Araya, Mitochondrial quality control in COPD and IPF, Cells 7 (2018) 86.
[38] I. Bellezza, I. Giambanco, A. Minelli, R. Donato, Nrf2-Keap1 signaling in oxidative and reductive stress, Biochim. Biophys. Acta Mol. Cell Res. 1865 (2018) 721–733.
[39] Q. Liu, Y. Gao, X. Ci, Role of Nrf2 and its activators in respiratory diseases, Oxid. Med. Cell. Longev. 2019 (2019) 1–17, https://doi.org/10.1155/2019/7090534, 7090534.
[40] A. Singh, et al., Nrf2-dependent sulfiredoxin-1 expression protects against cigarette smoke-induced oxidative stress in lungs, Free Radic. Biol. Med. 46 (2009) 376–386.
[41] K. Yamada, et al., Impaired nuclear factor erythroid 2-related factor 2 expression increases apoptosis of airway epithelial cells in patients with chronic obstructive pulmonary disease due to cigarette smoking, BMC Pulm. Med. 16 (2016) 27.
[42] K. Mizumura, S. Maruoka, T. Shimizu, Y. Gon, Role of Nrf2 in the pathogenesis of respiratory diseases, Respir. Investig. 58 (2020) 28–35.
[43] X.X. Lin, et al., Cigarette smoke extract-induced BEAS-2B cell apoptosis and anti-oxidative Nrf-2 up-regulation are mediated by ROS-stimulated p38 activation, Toxicol. Mech. Methods 24 (2014) 575–583.
[44] T. Sekine, T. Hirata, T. Mine, Y. Fukano, Activation of transcription factors in human bronchial epithelial cells exposed to aqueous extracts of mainstream cigarette smoke in vitro, Toxicol. Mech. Methods 26 (2016) 22–31.
[45] T. Sekine, et al., Regulation of NRF2, AP-1 and NF-κB by cigarette smoke exposure in three-dimensional human bronchial epithelial cells, J. Appl. Toxicol. 39 (2019) 717–725.
[46] R. Radi, Oxygen radicals, nitric oxide, and peroxynitrite: redox pathways in molecular medicine, Proc. Natl. Acad. Sci. USA 115 (2018) 5839–5848.
[47] Y. Su, W. Han, C. Giraldo, Y. De Li, E.R. Block, Effect of cigarette smoke extract on nitric oxide synthase in pulmonary artery endothelial cells, Am. J. Respir. Cell Mol. Biol. 19 (1998) 819–825.
[48] Z. Cui, et al., Involvement of calpain-calpastatin in cigarette smoke-induced inhibition of lung endothelial nitric oxide synthase, Am. J. Respir. Cell Mol. Biol. 33 (2005) 513–520.
[49] E. Ferrer, et al., Effects of cigarette smoke on endothelial function of pulmonary arteries in the Guinea pig, Respir. Res. 10 (2009) 76.
[50] W.F. Carlo, E. Villamor, N. Ambalavanan, J.G.R. DeMey, C.E. Blanco, Chronic exposure to cigarette smoke extract impairs endothelium-dependent relaxation of chicken embryo pulmonary arteries, Biol. Neonate 80 (2001) 247–250.
[51] J.L. Wright, A. Churg, Short-term exposure to cigarette smoke induces endothelial dysfunction in small intrapulmonary arteries: analysis using Guinea pig precision cut lung slices, J. Appl. Physiol. 104 (2008) 1462–1469.
[52] M. Tawa, et al., Impact of cigarette smoking on nitric oxide-sensitive and nitric oxide-insensitive soluble guanylate cyclase-mediated vascular tone regulation, Hypertens. Res. 43 (2020) 178–185.
[53] E.R. Derbyshire, M.A. Marletta, Structure and regulation of soluble guanylate cyclase, Annu. Rev. Biochem. 81 (2012) 533–559.
[54] R.C. Shah, S. Sanker, K.C. Wood, B.G. Durgin, A.C. Straub, Redox regulation of soluble guanylyl cyclase, Nitric Oxide - Biol. Chem. 76 (2018) 97–104.
[55] M.M. Rahaman, et al., Cytochrome b5 reductase 3 modulates soluble guanylate cyclase redox state and cGMP signaling, Circ. Res. 121 (2017) 137–148.
[56] B.G. Durgin, et al., Loss of smooth muscle CYB5R3 amplifies angiotensin II–induced hypertension by increasing sGC heme oxidation, JCI Insight 4 (2019), e129183.
[57] P. Sandner, et al., Soluble guanylate cyclase stimulators and activators, Handb. Exp. Pharmacol. 264 (2021) 355–394.
[58] N. Weissmann, et al., Stimulation of soluble guanylate cyclase prevents cigarette smoke-induced pulmonary hypertension and emphysema, Am. J. Respir. Crit. Care Med. 189 (2014) 1359–1373.
[59] A. Ghosh, et al., Soluble guanylate cyclase as an alternative target for bronchodilator therapy in asthma, Proc. Natl. Acad. Sci. U. S. A 113 (2016) E2355–E2362.
[60] (Government Laboratory - Tar and Nicotine Report).
[61] A.J. Valente, L.A. Maddalena, E.L. Robb, F. Moradi, J.A. Stuart, A simple ImageJ macro tool for analyzing mitochondrial network morphology in mammalian cell culture, Acta Histochem. 119 (2017) 315–326.
[62] S. Creed, M. McKenzie, Measurement of mitochondrial membrane potential with the fluorescent dye tetramethylrhodamine methyl ester (TMRM), Methods Mol. Biol. (1928) 69–76, 2019.
[63] R.F. Hoffmann, et al., Prolonged cigarette smoke exposure alters mitochondrial structure and function in airway epithelial cells, Respir. Res. 14 (2013).
[64] B. Aravamudan, et al., Cigarette smoke-induced mitochondrial fragmentation and dysfunction in human airway smooth muscle, Am. J. Physiol. Lung Cell Mol. Physiol. 306 (2014).
[65] B. Aravamudan, et al., Functional effects of cigarette smoke-induced changes in airway smooth muscle mitochondrial morphology, J. Cell. Physiol. 232 (2017) 1053–1068.
[66] S. Dikalov, Cross talk between mitochondria and NADPH oxidases, Free Radic. Biol. Med. 51 (2011) 1289–1301.
[67] A. Daiber, et al., Crosstalk of mitochondria with NADPH oxidase via reactive oxygen and nitrogen species signalling and its role for vascular function, Br. J. Pharmacol. 174 (2017) 1670–1689.

[68] B. Zhuan, et al., Hypoxia induces pulmonary artery smooth muscle dysfunction through mitochondrial fragmentation-mediated endoplasmic reticulum stress, Aging 12 (2020) 23684–23697.
[69] S. Ito, et al., PARK2-mediated mitophagy is involved in regulation of HBEC senescence in COPD pathogenesis, Autophagy 11 (2015) 547–559.
[70] F. Li, et al., Roles of mitochondrial ROS and NLRP3 inflammasome in multiple ozone-induced lung inflammation and emphysema, Respir. Res. 19 (2018) 230.
[71] M.J. Rossman, et al., Chronic supplementation with a mitochondrial antioxidant (MitoQ) improves vascular function in healthy older adults, Hypertens. 71 (1979) 1056–1063, 2018.
[72] K.B. Neves, et al., Peripheral arteriopathy caused by Notch3 gain-of-function mutation involves ER and oxidative stress and blunting of NO/sGC/cGMP pathway, Clin. Sci. (Lond). 135 (2021) 753–773.